Real-Time Ion-Flux Imaging in the Growth of Micrometer-Scale Structures and Membranes

Balazs Nemeth, Mark D. Symes, Antoine G. Boulay, Christoph Busche, Geoffrey J. T. Cooper, David R. S. Cumming, and Leroy Cronin**

Monitoring ion fluxes in natural[1] and artificial[2] systems is a fundamental area of research in medicine and nanoscience. However, methods for obtaining time-resolved data which correlate ionic movements on the nanometer-scale with events at the micro-scale remain elusive. Herein, we use an ion-sensitive field-effect transistor (ISFET)[3] device coupled with optical microscopy to simultaneously image the growth of, and ion flux through, micrometer-scale tubes and membranes built from nanometer-scale polyoxometalate (POM) clusters.[4] An excellent correlation is observed between the optical and ionic imaging data, showing that the ISFET arrays give high resolution spatial and temporal information regarding the initiation and rate of ionic movements. The small size of the ISFET devices and their ability to track ionic movements in a time-resolved and non-destructive manner exemplifies their extraordinary potential for monitoring non-equilibrium ion fluxes in processes as diverse as biomineralization,[5] intracellular transport processes,[6] molecular self-assembly[7] and synthetic biology.[8]

ISFET sensory arrays (ISAs) with varying ion-selective surfaces have found a large range of applications in the biochemical[9] and medical sciences.[10–12] In addition, ISFETs display excellent real-time data acquisition rates, which should allow improved temporal resolution of ion fluxes. On account of this, and motivated by a desire to probe the mechanisms behind ion-pair recognition[13] and self-assembly in complex emergent chemical processes,[14,15] we investigated the ion-sensing capabilities of ISFET devices during the non-equilibrium self-assembly of POM-based tubes[16–18] and membranes,[15] using simultaneous optical microscope video imaging to assess the performance of the ISA. Herein, we report on our findings, and show that it is indeed possible to correlate the trajectories traced by individual growing tubes (and membranes) as seen with the optical microscope with the read-out of the ISA, giving a complementary metal-oxide-semiconductor (CMOS)[21,22]-based lab-on-a-chip ion camera system. By suitable data processing, it was possible to view both the relative global ion concentration in a system and the areas of highest rate of change of ion concentration, at the growing edges of tubes and membranes. This allowed us to image and quantify the real-time self-assembly of complex micrometer-scale structures from nanoscale precursors by looking at signature changes in the overall ion flux; a technique we term *Ionic Mapping*. To the best of our knowledge, this work constitutes the first example of the in situ micrometer-scale monitoring and imaging of the spatial and temporal distribution of an out-of-equilibrium ion gradient using ISFETs, with enormous implications for examining and harnessing emergent processes, and both mapping and controlling the growth of micro-structured materials that result from such non-equilibrium systems.[21,22]

The growth mechanism of polyoxometalate tubes and membranes explored herein using the ISFET array is shown in **Figure 1**. Taking the example of tubes, growth occurs when an aqueous solution containing a sparsely-soluble organic cation is placed on top of a crystal of an equally poorly-soluble polyoxometalate (Figure 1A). Upon solution-crystal contact, the crystal slowly and partially dissolves in the aqueous solution, releasing polyoxometalate anions and their supporting counter-cations (e.g., H^+ and Na^+). When the POM anions encounter the rather insoluble organic cations in solution, the two immediately precipitate as an insoluble ion-pair producing a hollow membrane around the crystal (Figure 1B). This membrane is, however, permeable to water molecules, which thus pass from solution into the more concentrated space inside the membrane, causing the osmotic pressure to increase. When the system reaches a critical pressure, the membrane ruptures (Figure 1C), and dissolved POM material within the membrane is forced through the aperture into the cation solution, leading to further aggregation. As water ingress through the membrane surrounding the crystal maintains a constant outflow of material through the opening, the structure cannot close-up and so continued aggregation produces extended tubular architectures (Figure 1D). These continue to grow until all the dissolved polyoxometalate material within the membrane has been exhausted, at which point the osmotic pressure driving tube formation drops and the ends of the tubes close up.

In an attempt to map the ion flux at the mouth of a growing polyoxometalate tube, we used a square-shaped 64 × 64-pixel ISA system, containing 4096 individual sensors (each of dimension 10.2 μm × 10.2 μm) to image the growth of tubes of micrometer-scale diameter on the surface of the Si_3N_4 ion-sensing layer of the array (see Supporting Information for details of ISA design and operation). As pixels are capable of registering a signal independently of their neighboring pixels, this means

B. Nemeth, Prof. D. R. S. S. Cumming
Electronics Design Centre, School of Engineering
University of Glasgow
G12 8LT, UK
E-mail: David.Cumming.2@glasgow.ac.uk
Dr. M. D. Symes, A. G. Boulay, Dr. C. Busche, Dr. G. J. T. Cooper, Prof. L. Cronin
WestCHEM, Department of Chemistry
University of Glasgow, G12 8QQ, UK
E-mail: L.Cronin@chem.gla.ac.uk

DOI: 10.1002/adma.201104345

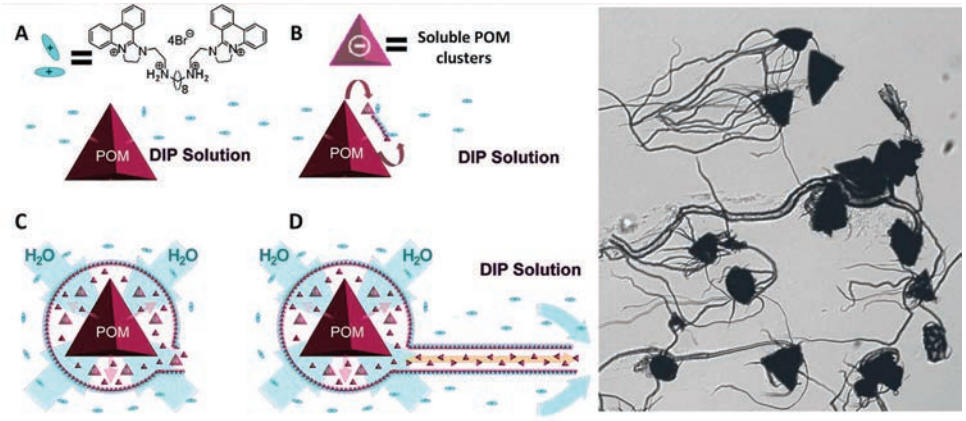

Figure 1. LHS: Mechanism of growth of polyoxometalate tubes and membranes. A: a solution containing a sparsely-soluble organic cation (bis-DIP in this instance, vide infra) is placed on top of the polyoxometalate crystal. B: a membrane of polyoxo-anions and organic cations forms. C: the osmotic pressure rises inside the water-permeable membrane, which then ruptures. D: after membrane rupture, tube growth is powered by osmotic pressure within the membrane. RHS: Optical microscope image showing tubular architectures grown from crystals of a polyoxometalate.

that the minimum spatial resolution that the ISA can provide is ±10.2 μm on any particular feature. This is, however, sufficient to observe changes in the width of polyoxometalate-based tubes as a function of the concentration of the counteraction (vide infra). Each pixel had a minimum stable data acquisition time of 40 μs, and pixels were read sequentially in blocks of 256, giving a fastest total sampling rate of 10.2 ms per frame, or around 100 frames per second (FPS) on 16 analog channels simultaneously. Hence, in this configuration, the ionic environment at any given pixel is sampled once every 10.2 ms. In all, the area occupied by the ISA was 715.8 μm × 715.8 μm. Sealing the surrounding circuitry with resistant epoxy (Epotek 302-3M) and incorporation of a robust polypropylene container gave a watertight array suitable for monitoring solution-phase self-assembly processes (see **Figure 2** and Figures S3-S5). The experiments performed in this work were all conducted in aqueous solution, at room temperature and no attempts were made to exclude air or ambient light. Whilst silicon-based ISFETs such as the current device do show a response to intense light sources, we did not detect any effect of light on the ISFETs at the low light levels extant in our laboratory. Moreover, we did not detect any noticeable reduction in performance of the ISA over the pH range employed (1-12). However, we performed no systematic study of the effect of *non-aqueous* solvents on the stability of the ISFET array.

Initially, the sensitivity of the ISA to changes in the concentration of H^+ (pH 1–12) and Na^+ (pNa 0–4) in solutions in contact with the array passivation layer was ascertained, giving sensitivities of ~20 mV/pH unit and ~9 mV/pNa unit - see Figures S6 and S7. Given this sensitivity (the smallest voltage change that can be resolved by the ISA is approximately 500 μV),[9] we reasoned that the array should be able to detect H^+ and Na^+ expelled from the growing mouth of tubes formed from crystals of the polyoxometalate $Na_4H_3(C_6H_{11}N_2)_{13}[(SiW_{10}O_{36})_2(Ni_4O_6)]\cdot 12H_2O$ (POM-1) immersed in aqueous solutions of organic cations. The organic cation used was *N,N´*-bis(5-phenanthridinium-5-yl-ethyl chloride)octane-1,8-diamine dihydrochloride (bis-DIP), which has previously been shown to create well-defined tubular structures with POM-1.[18] Initially, we placed 1 mL of a 2.5 mM solution of bis-DIP onto the ISA, and allowed the voltage read-out from the ISFET to stabilize (typically 2-5 minutes). After this time, small (~0.1 mm × 0.1 mm × 0.1 mm) crystals of POM-1 were placed manually onto the Si_3N_4 surface of the sensor array using the tip of a needle, such that the crystals did not float on top of the bis-DIP solution, but rested on the Si_3N_4 surface. Due to the small surface area of the ISA, only a very few of the crystals placed on the chip fell on the ion-sensitive area. However, those crystals which did fall on the ISA soon gave rise to membranous morphologies. **Figure 3** shows the growth of membranes from a crystal of POM-1 in 2.5 mM bis-DIP at various time intervals. The grey photographs on the left hand side were taken using the optical microscope, the center column gives colored "ion maps" showing the ion-sensitive read-out of the ISFET and the right hand column gives the analog voltage outputs recorded by four selected pixels on the path of the growing membrane (the positions of these pixels are marked in time and space with black arrows on Figure 3). The calibration curves for both protons and sodium ions (Figures S6 and S7 respectively) show that a given voltage read-out at a pixel corresponds to a given ionic strength in the solution covering that pixel. In order to generate the ions maps shown herein, the read-out from the entire ensemble of pixels was then translated into a color scheme, and hence the ion maps show quantitative data in a graphical manner. Both ISA-derived sets of data were corrected for fixed pattern noise by subtracting a single common reference frame from the raw data, so that changes in the ion concentration showed up with sufficient contrast from background noise (see Supporting Information for details). This reference data represents a 64 × 64 matrix of acquired sensor output voltages that was collected before the crystals were placed on the array, when the ISA read-out was essentially invariant (i.e., before t = 14.6 s from the right hand column of Figure 3).

The two different ion camera data representations in Figure 3 highlight different aspects of the membrane growth. The ion maps in the central column display the overall concentration

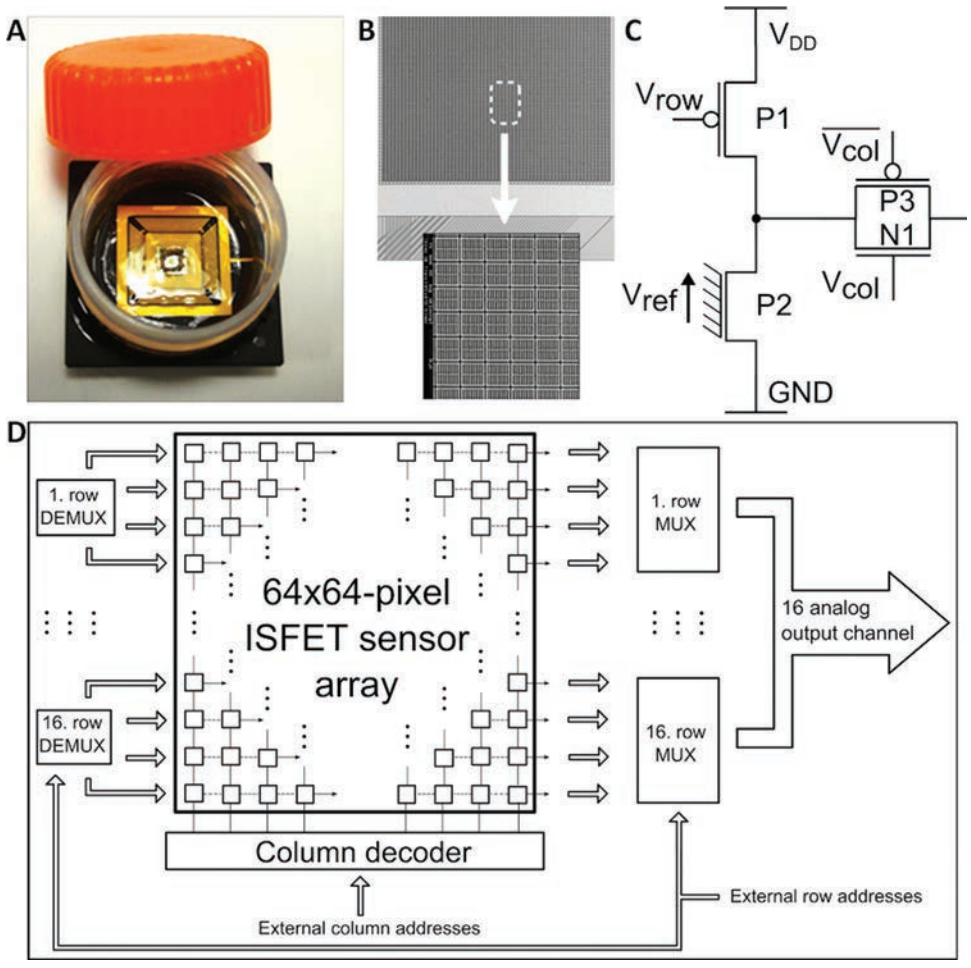

Figure 2. The 64 × 64-pixel ISA showing the water-tight reaction chamber (A) and a close-up of the array as viewed by SEM (B). The magnification is ×134 for the whole array and ×1972 for the expanded image. C: a circuit schematic of the ISFET array and (D) a pictorial representation of the method used for the automated data acquisition sequence (see Supporting Information for details).

of Na^+ and H^+ within the expanding membrane as a whole, allowing us to see that the concentration of ions is higher inside the sack than in the solution in general, and that within this sack, the ion concentration is highest nearest the crystal. The single pixel voltage difference versus time graphs (right hand column) show how the read-out of a pixel changes as the membrane grows over the top of that pixel. In all four of these graphs, a large increase in the voltage read-out of the pixels is recorded at $t = 14.6$ s, which corresponds to the time at which crystals of POM-1 were placed onto the surface of the array: clearly the crystal starts to dissolve immediately, releasing ions which the ion camera detects. However, membrane formation also occurs very rapidly. Taking the data displayed in the right hand column of Figure 3A, we notice an inflection point in the voltage-difference vs. time graph after the initial rise in values brought about by crystal immersion. This point of inflection ($t = 17.1$ s), corresponds to the time at which the membrane edge reaches the pixel in question (see black cross and arrow on the ion map and the excellent agreement with the optical data in Figure 3A). The voltage read-out from that pixel then increases again, before leveling out at a constant level indicative of a higher concentration of ions on that pixel compared to the baseline. This pattern is repeated at each of the other three pixels shown in Figure 3 as the membrane grows over them, and indeed the point of inflection corresponding to the time the membrane edge reaches these pixels gets more distinct (even if the voltage read-out is lower in absolute terms) the further away from the crystal those pixels are. Hence both the elevated ion concentration within the membrane sack and the position of the leading edge of the expanding membrane can be visualized, seemingly with excellent correlation to the data obtained by the optical microscope. It should be noted at this stage that the ISA will only give a response if the ionic concentration changes *on the surface of the array*. Hence an ion map gives a two-dimensional picture of how the growing membrane sits on the Si_3N_4 surface: although the membrane is almost certainly growing outwards from the crystal in all directions, the ISA only records growth along its interface with the membrane. However, Figure 3 also suggests that ionic mapping can give information on processes that cannot be detected using the optical microscope. Comparing the ion maps in the central column of Figure 3 with the optical microscope images, we see

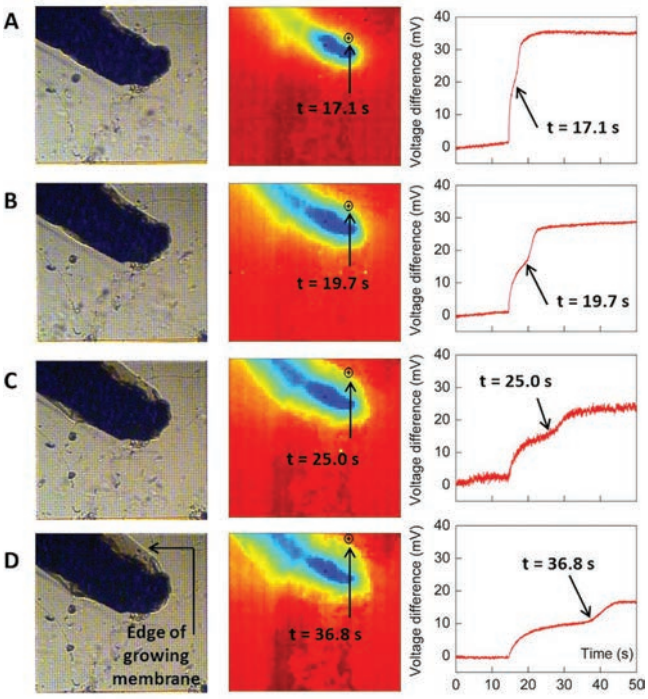

Figure 3. Membrane growth from a crystal of POM-1 in 2.5 mM bis-DIP at various times after placement of the crystal on the surface of the ISA. Images from left to right are as follows: photographs taken using an optical microscope (left hand column); ion camera read-outs showing the overall H^+/Na^+ concentration (center column, areas of higher ISA read-out - higher ion concentration/concentration change - are given in blue; areas of lower activity are in red); and single pixel voltage-difference *vs.* time read-outs for the growing membrane which highlight the edge of the growing membrane as labeled points of inflection in the curves. The membrane expanded a distance of 10 pixels between the black crosses indicating t = 17.1 s and t = 36.8 s. The shortest route across a pixel is 11.2 µm (one 10.2 µm pixel side plus an inter-pixel gap of 1 µm), hence the total distance the membrane expanded in this direction was 10 × 11.2 µm = 0.11 mm. This corresponds to a membrane growth rate of approximately 5.7 μms^{-1} in this vector, although we note that membrane expansion does not appear to be uniform in all directions. The size of the array shown in all panels is 57 × 57 pixels. The time resolution of recording was 400 µs/pixel and 102.4 ms/complete frame, or around one tenth of the maximal sampling rate of the system.

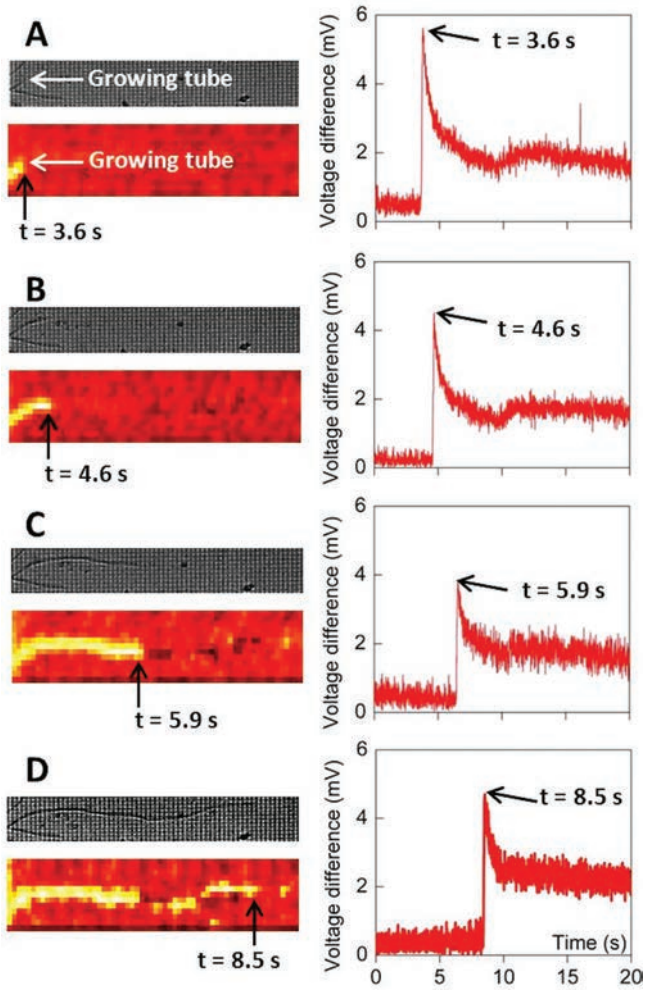

Figure 4. Tube growth from a crystal of POM-1 in 10 mM bis-DIP at various times after the tube reaches the edge of the ISA. The top panels in the left hand column of Figures 4A-4D were taken using an optical microscope, whilst the lower panels in the left hand column are the read-outs from the ISA device (colors chosen to maximize contrast for clarity: yellow indicates high ion concentration and red low concentration). The size of these slices is ~64 × 11 pixels. The right hand column shows voltage difference *vs.* time curves for individual pixels on the path of the growing tube. The positions of these pixels are given by the arrows on the ion maps in the left hand column. The diameter of the tubes by optical microscopy is approximately one pixel (~11 µm), whilst the ISA gives a slightly less resolved signal roughly two pixels wide. The tube travelled ~56 pixels (or 11.2 µm × 56 = 0.63 mm) in ~4.9 s, giving a growth rate of ~130 µm/s. The time resolution of recording was 40 µs/pixel and 10.2 ms/complete frame, the maximal sampling rate of the system.

that there is only very low ionic activity registered in the upper left hand corner of the ion maps, whilst the optical microscope shows this area to be covered by the crystal (where a high concentration of ions would otherwise be expected). This suggests that the upper left hand part of the crystals may not in fact be in direct contact with the surface of the ISA, information that it is not possible to obtain using the optical microscope images alone. Furthermore, it is also informative to note the high sensitivity of the ISA to the localized small variations in pH and pNa that are occurring during membrane growth: a high-sensitivity Mettler Toledo SevenMulti pH meter failed to detect any variation in pH in the bulk solution during membrane growth, whereas the changes in effective ion concentration on the surface were clearly resolved by the ISA.

The growth of tubular structures could also be monitored using the dual optical microscope/ion camera apparatus. In order to achieve tube, rather than membrane formation, the concentration of the organic cation was increased, in line with previous tube-growing experiments with POM-1 and bis-DIP.[18] **Figure 4** shows the growth of a tube on the surface of the array, both by optical microscope (Figures 4A-D, upper panels of left hand column), and ISA ion map (Figures 4A-D, lower panels of left hand column: the reference frame for all the ISA data in Figure 4 was again taken before the crystals were immersed in the bis-DIP solution). In Figure 4A, a tube originating from a crystal not on the ISA and outside the field of view of the

optical microscope reaches the edge of the sensory array area. This tube then grows across the array over the next 5 seconds (Figures 4B-D). The analog voltage outputs recorded by four selected pixels on the path of the tube are shown in the right hand column of Figure 4 (black arrows on the ion maps indicate the positions of these pixels). The resulting voltage difference vs. time graphs show how the read-out of a pixel changes as the tube grows over the top of that pixel. Taking the example of the data in Figure 4A, we find that the pixel has a baseline voltage read-out until t = 3.6 s, at which point the growing end of the tube passes over that pixel. A sharp spike in read-out is recorded initially, which dies away over ~4 s. The read-out from the pixel then remains constant, at a level indicating a higher concentration of H^+ and Na^+ on that pixel compared to the baseline, i.e., compared to the situation before the tube grew over the pixel. This pattern is repeated at each of the other three pixels in the path of the tube shown in Figure 4 as the tube passes over those pixels. The presence of a sharp spike in the voltage-difference vs. time read-outs (compared to just the gentle bumps seen in the curves in Figure 3) is a consequence of the faster rate of growth (and hence change in ion flux) associated with tubes compared to membranes. Indeed, the tube in Figure 4 grows over twenty times faster than the membrane in Figure 3. Thus the rate of change in capacitance on the nitride surface produced by tubes growing over a pixel is far greater than that produced by slower membrane growth, giving a more pronounced transient response in the voltage-difference versus time curves. Further tube-growing experiments are reported in the Supporting Information (Figure S8).

The examples of ionic mapping shown in this paper all have corresponding optical microscopy images, to give some sense of calibration as to the efficacy with which the ISA detects ion fluxes in both space and time. In this regard, the work described herein demonstrates that both spatially and temporally, the read-out from the ISA is a very accurate representation of tube and membrane growth. Indeed, in practice, the ISA was able to give high-fidelity data on the growth and morphology of tubes and membranes on the surface of the array that were otherwise obscured from the view of the optical microscope (as suggested by Figure 3, for example). As many of the potential applications of ion mapping are in systems and environments where optical monitoring of ion fluxes may be impractical or impossible, the independent data provided by such ISAs promises to be a transformative analytical tool with immediate application in exploring the growth of ionic materials.

In summary, we have demonstrated the use of coupled optical and ionic mapping techniques to monitor the growth of micrometer-scale inorganic tubes and membranes, and hence to prove the utility of ISAs for monitoring ion fluxes in systems where other techniques cannot be used. Moreover, it was possible to display not only the global ionic concentrations associated with these structures, but also to identify the regions in which the ionic flux was changing most rapidly, at the growing ends of tubes and at the expanding boundaries of membranes. To our knowledge, this is the first demonstration of an ISFET platform for the simultaneous spatial and temporal resolution of ion fluxes in the growth of real materials, with implications wherever non-equilibrium ion fluxes are important, throughout the chemical and life sciences.

Acknowledgements

We thank the EPSRC (UK) for funding and Roslyn Eadie (University of Glasgow) for samples of bis-DIP. DRSC and LC thank the Royal Society/ Wolfson Foundation for merit awards.

Received: November 12, 2011
Revised: January 4, 2012
Published online: January 30, 2012

[1] F. M. Ashcroft, *Nature* **2006**, *440*, 440.
[2] P. A. Gale, *Acc. Chem. Res.* **2011**, *44*, 216.
[3] P. Bergveld, *IEEE T. Bio-Med. Eng.* **1970**, *17*, 70.
[4] D.-L. Long, R. Tsunashima, L. Cronin, *Angew. Chem. Int. Ed.* **2010**, *49*, 1736.
[5] Y.-Y. Kim, K. Ganesan, P. Yang, A. N. Kulak, S. Borukhin, S. Pechook, L. Ribeiro, R. Kröger, S. J. Eichhorn, S. P. Armes, B. Pokroy, F. C. Meldrum, *Nat. Mater.* **2011**, *10*, 890.
[6] S. Soh, M. Byrska, K. Kandere-Grzybowska, B. A. Grzybowski, *Angew. Chem. Int. Ed.* **2010**, *49*, 4170.
[7] T. Liu, M. L. K. Langston, D. Li, J. M. Pigga, C. Pichon, A. M. Todea, A. Müller, *Science* **2011**, *331*, 1590.
[8] A. Müller, S. K. Das, S. Talismanov, S. Roy, E. Beckmann, H. Bögge, M. Schmidtmann, A. Merca, A. Berkle, L. Allouche, Y. Zhou, L. Zhang, *Angew. Chem. Int. Ed.* **2003**, *42*, 5039.
[9] J. M. Rothberg, W. Hinz, M. Rearick, J. Schultz, W. Mileski, M. Davey, J. H. Leamon, K. Johnson, M. J. Milgrew, M. Edwards, J. Hoon, J. F. Simons, D. Marran, J. W. Myers, J. F. Davidson, A. Branting, J. R. Nobile, B. P. Puc, D. Light, T. A. Clark, M. Huber, J. T. Branciforte, I. B. Stoner, S. E. Cawley, M. Lyons, Y. Fu, N. Homer, M. Sedova, X. Miao, B. Reed, J. Sabina, E. Feierstein, M. Schorn, M. Alanjary, E. Dimalanta, D. Dressman, R. Kasinskas, T. Sokolsky, J. A. Fidanza, E. Namsaraev, K. J. McKernan, A. Williams, G. T. Roth, J. Bustillo, *Nature* **2011**, *475*, 348.
[10] P. A. Hammond, D. Ali, D. R. S. Cumming, *IEEE T. Bio-Med. Eng.* **2005**, *52*, 687.
[11] M. J. Milgrew, M. O. Riehle, D. R. S. Cumming, *Sensor. Actuators B* **2005**, *111-112*, 347.
[12] M.-I. Mohammed, M. P. Y. Desmulliez, *Lab Chip* **2011**, *11*, 569.
[13] S. K. Kim, J. L. Sessler, *Chem. Soc. Rev.* **2010**, *39*, 3784.
[14] R. K. Kumar, X. Yu, A. J. Patil, M. Li, S. Mann, *Angew. Chem. Int. Ed.* **2011**, *50*, 9343.
[15] G. J. T. Cooper, P. J. Kitson, R. Winter, M. Zagnoni, D.-L. Long, L. Cronin, *Angew. Chem. Int. Ed.* **2011**, *50*, 10373.
[16] C. Ritchie, G. J. T. Cooper, Y.-F. Song, C. Streb, H. Yin, A. D. C. Parenty, D. A. MacLaren, L. Cronin, *Nat. Chem.* **2009**, *1*, 47.
[17] G. J. T. Cooper, L. Cronin, *J. Am. Chem. Soc.* **2009**, *131*, 8368.
[18] G. J. T. Cooper, A. G. Boulay, P. J. Kitson, C. Ritchie, C. J. Richmond, J. Thiel, D. Gabb, R. Eadie, D.-L. Long, L. Cronin, *J. Am. Chem. Soc.* **2011**, *133*, 5947.
[19] E. M. Vogel, *Nat. Nanotechnol.* **2007**, *2*, 25.
[20] R. Chau, B. Doyle, S. Datta, J. Kavalieros, K. Zhang, *Nat. Mater.* **2007**, *6*, 810.
[21] T. Bansagi, Jr., V. K. Vanag, I. R. Epstein, *Science* **2011**, *331*, 1309.
[22] N. Hiroya, A. S. Mikhailov, *Nat. Phys.* **2010**, *6*, 544.